Local Viscosity Change in Water near a Solid-Liquid Interface and its Extraction by Means of Molecular Rotational Diffusion – a Molecular Dynamics Study –

Satoshi Nakaoka[a], Donatas Surblys[a], Yasutaka Yamaguchi[a,*], Koji Kuroda[b], Tadashi Nakajima[b], Hideo Fujimura[b]

[a]*Department of Mechanical Engineering, Osaka University, 2-1 Yamadaoka, Suita 565-0871, Japan*
[b]*R & D Center, Dai Nippon Printing Co., Ltd., 1-1-3 Midorigahara, Tsukuba 300-2646, Japan*

Abstract

The relation between the rotational diffusion (RD) coefficient of water molecules and viscosity, that theoretically are inversely proportional to each other, was examined by using molecular dynamics simulations. In a homogeneous bulk liquid system, both the viscosity calculated from the virial theorem and the experimental one correlated well with the inverse of water RD coefficient at various temperatures. In a heterogeneous system of water between solid walls with different solid-liquid interaction strength, the viscosity distribution was similar to the distribution of the RD coefficient inverse multiplied by density, and this suggests the possibility of extracting nanometer-scale viscosity distribution by RD.

Keywords: Molecular Dynamics, Rotational Diffusion, Viscosity, Solid-Liquid Interface

1. Introduction

Liquid motion on solid surfaces has long been a topic of interest in various fields because of its considerable practical importance, and with the

*Corresponding author
Email addresses: nakaoka@gcom.mech.eng.osaka-u.ac.jp (Satoshi Nakaoka), donatas@gcom.mech.eng.osaka-u.ac.jp (Donatas Surblys), yamaguchi@mech.eng.osaka-u.ac.jp (Yasutaka Yamaguchi)

development of manufacturing and measurement technology it has become particularly essential in microscale devices, sensors as well as biological flow. For instance, recent length scale of semiconductor chips has been reduced down to a few tens of nanometers, and profound understanding of nanoscale liquid behavior on a solid surface in the fabrication or cleaning processes is a key issue for controlling the resulting quality.

In sub-nanometer scale, liquid behavior as a continuum is violated by the motion of discrete molecules and is especially remarkable when the molecular motion is anisotropically constrained due to the nonspherical molecular structure and/or liquid-liquid and liquid-solid interactions. A typical example is water flow in a carbon nanotube (CNT) [1, 2, 3]. A large velocity slip between water and a CNT was indicated, which was very different from that in a non-slip macroscale flow, and through molecular dynamics (MD) simulations and experiments [4, 5, 6, 7, 8], this feature was attributed to the peculiar order of water molecules confined in nanometer space.

Although the flow in a CNT is a rather extreme case, effects of the velocity slip at the solid-liquid interface indeed become considerable in microscale liquid motion. MD simulations of the liquid slip have been carried out for a simple molecular model as well [9], and understanding at molecular scale based on MD simulations is well reviewed in Ref. [10]. In any case, extracting local dynamic properties in nanometer scale should be important for further analysis on slip behavior.

Regarding the motion of liquid molecules near the solid surface, we have carried out MD simulations of a single water droplet on a solid surface [11] in order to investigate the wetting behavior. In that study, it was shown that the change of local dynamic property of water molecules near the solid surface with different solid-liquid interaction parameters was clearly captured through the distribution of rotational diffusion (RD) coefficient, which was calculated from the time evolution of the angular displacement of molecular principal axes. On the other hand, the difference was not apparently reflected in the distribution of hydrogen-bond lifetime.

In respect to diffusion, the translational diffusion (TD) coefficient of a spherical particle D_t is correlated to viscosity as

$$D_t = \frac{kT}{6\pi\mu R_t}, \tag{1}$$

where μ, R_t, k and T denote the viscosity, effective particle radius for translational motion, Boltzmann constant and temperature, respectively. This is

known as the Stokes-Einstein equation [12]. Similarly, the RD coefficient D_r is theoretically inversely proportional to the viscosity through the Stokes-Einstein-Debye relation [12]:

$$D_r = \frac{kT}{8\pi\mu R_r^3}, \tag{2}$$

where R_r is the effective particle radius for rotational motion. The relation in Eq. (2) is originally derived for the Brownian motion of a microscale particle constrained onto a sphere in a fluid. However, if this can be extended and is also applicable to the molecular rotational motion, the distribution of RD coefficient in our previous study [11] may have expressed nanoscale viscosity distribution. Because the rotational motion of water molecule is faster than the translational motion, i.e. RD has a much shorter timescale than TD, it is possible to obtain the spatial distribution of RD coefficient with higher resolution. In addition, extracting the local diffusivity through the water RD coefficient is possible even near the solid surface because its rotation is not highly constrained there due to its mostly spherical shape. On the other hand, it is difficult to extract local diffusivity through the TD coefficient because the position displacement in space is restricted and therefore not isotropic. Thus, this method to extract local distribution of RD coefficient can be a potentially efficient tool to obtain nanometer-scale local liquid properties of pure water or water mixture.

Although both diffusion coefficients D_t and D_r are theoretically inversely proportional to the viscosity μ as in Eqs. (1) and (2) [13], it has not been confirmed yet whether the latter relation between RD coefficient of component molecules and fluid viscosity also holds locally. In this study, MD simulations are at first performed in order to investigate this D_r-μ relation in terms of the temperature dependence of RD coefficient and viscosity in a homogeneous bulk liquid system. Furthermore, the D_r-μ relation is also examined in a heterogeneous water system between solid walls in terms of local distributions.

2. Method

2.1. Potential model

The potential model is the same as in our previous study [11]. Water molecule expressed by the SPC/E [14] potential model is adopted as the fluid

component. The 12-6 L-J and Coulomb potentials are assumed as the intermolecular interactions between hydrogen and oxygen atoms, respectively as in Eqs. (3) and (4):

$$\Phi^{\mathrm{LJ}}(r_{ij}) = H(r_c - r_{ij}) \cdot 4\epsilon_{ij} \left[\left(\frac{\sigma_{ij}}{r_{ij}} \right)^{12} - \left(\frac{\sigma_{ij}}{r_{ij}} \right)^{6} + \left\{ c_2^{\mathrm{LJ}} \left(\frac{r_{ij}}{r_c} \right)^2 - c_0^{\mathrm{LJ}} \right\} \right], \quad (3)$$

$$\Phi^{\mathrm{C}}(r_{ij}) = H(r_c - r_{ij}) \frac{q_i q_j}{4\pi\epsilon_0} \left[\frac{1}{r_{ij}} + \frac{1}{r_c} \left\{ c_2^{\mathrm{C}} \left(\frac{r_{ij}}{r_c} \right)^2 - c_0^{\mathrm{C}} \right\} \right], \quad (4)$$

where r_{ij} is the distance between positions of hydrogen or oxygen i and j, and ϵ_{ij}, σ_{ij}, q_i and ϵ_0 denote the L-J energy and length parameters, point charge at site i, and vacuum permittivity, respectively. These interactions in Eqs. (3) and (4) are rounded off at a cut-off distance r_c using the Heaviside step function H, and a quadric function is appended so that the potential smoothly becomes zero at $r_{ij} = r_c$. The cut-off distance r_c is set as 1.5 nm in this study, and the values of c_2^{LJ}, c_0^{LJ}, c_2^{C} and c_0^{C} are noted in Ref. [11].

An fcc crystal is assumed as the solid wall for the water-wall system, and interaction between nearest neighbors is expressed by the following harmonic potential:

$$\Phi^{\mathrm{H}}(r_{ij}) = \frac{k}{2} (r_{ij} - r_0)^2, \quad (5)$$

where r_0 and k denote the equilibrium distance and spring constant, respectively. Values of a platinum crystal are used for the lattice constant and mass of the solid atom as well as for van der Waals radius which is used for the solid-liquid interaction described below.

The interaction between fluid and solid particles is also expressed by the L-J potential working between oxygen and wall atoms. The length parameter $\sigma_{\mathrm{O-wall}}$ between oxygen and wall atoms is given by the Lorentz-Berthelot mixing rule $\sigma_{\mathrm{O-wall}} = (\sigma_{\mathrm{O-O}} + \sigma_{\mathrm{wall-wall}})/2$, in which the van der Waals radius of a platinum crystal is referred for $\sigma_{\mathrm{wall-wall}}$. On the other hand, the energy parameter $\epsilon_{\mathrm{O-wall}}$ is set as a calculation parameter by multiplying the fluid-solid interaction coefficient η to a base value $\epsilon^0_{\mathrm{O-wall}}$ as $\epsilon_{\mathrm{O-wall}} = \eta \cdot \epsilon^0_{\mathrm{O-wall}}$. The base value $\epsilon^0_{\mathrm{O-wall}}$ was empirically defined to give an approximately 90° contact angle at $\eta = 1.2$ when a water droplet is positioned on the solid surface [11].

The potential and mass parameters are summarized in Table 1.

2.2. Simulation systems

The bulk liquid water system consists of 1200 water molecules in a cubic cell of a side length about 3.3 nm with periodic boundary condition in all directions. All data are obtained as the temporal average of 10 ns in a system under constant NVE condition, which is achieved after a preliminary equilibration under constant NPT condition [15] at each control temperature T_c between 280 and 320 K with atmospheric pressure.

The heterogeneous simulation system of liquid water between solid surfaces is exhibited in Fig. 1. Water molecules are confined between solid walls, where fcc (111) surfaces of solid crystal consisting of three layers are located at the bottom and top of the calculation cell with periodic boundary conditions in x- and y-directions. Each surface consists of 462 solid atoms and the side lengths in x- and y-directions are 3.1 and 3.4 nm. Both surfaces have the same solid-liquid interaction energy parameter $\epsilon_{\mathrm{O-wall}}$ and the system can be regarded as quasi-plane-symmetric in z-direction. The system height is about 5.5 nm and the number of water molecules is between 1362 and 1454, where the latter has been set so that the resulting pressure becomes approximately that of atmospheric pressure in each system with different $\epsilon_{\mathrm{O-wall}}$. Although as previously mentioned, some parameters of platinum crystal are used for the atoms of solid wall, the system can be considered as a simplified model-solid with varying solid-liquid interaction energy.

The positions of atoms in the outmost layers are fixed and the temperature of atoms in the middle layers is controlled by the Langevin method at 300 K with a Debye temperature of 240 K, while the inter-wall distance is varied by exerting an external force on the top wall during the equilibration run to obtain an equilibrium system at atmospheric pressure [16].

The velocity Verlet method with modified quaternion-constraint techniques [17, 18] is applied for the integration of the Newton's equation of motion with a time step Δt of 1 fs. All data are obtained as the temporal average of 24 ns for an equilibrium system after preliminary equilibration over 2 ns, where the calculation time is set to reproduce a reliable statistic average [19].

3. Results and Discussion

3.1. Temperature dependence of diffusion coefficients and viscosity in homogeneous bulk system

Figure 2 shows the time development of the mean square position displacement of center of mass $\langle|\Delta\vec{r}|^2\rangle$ and the mean square angular displacement of principal axes $\langle\Delta s^2\rangle$ of water molecule in a bulk system at $T = 300$ K. The brackets denote spatio-temporal average for all water molecules in the system and the average for three principal axes is exhibited for the mean square angular displacement. The calculation details of the angular displacement Δs that is not restricted below π are described in our previous work [11]. First-order fitting for the range from 2 to 7 ps is shown by the dotted lines from which TD coefficient D_t and RD coefficient D_r are respectively calculated in the Einstein form as

$$D_t = \frac{1}{6}\frac{d\langle|\Delta\vec{r}|^2\rangle}{dt} \tag{6}$$

and

$$D_r = \frac{1}{4}\frac{d\langle\Delta s^2\rangle}{dt}. \tag{7}$$

As highlighted in the lower right panel, both the position and angular displacements are on straight lines, i.e. the motion of water molecules loses ballistic behavior and shows diffusive feature after at most 2 ps. Specifically, the angular displacement in the main panel seems to reach diffusive behavior within about 1 ps, and this time is much shorter than that for the position displacement. This difference is attributed to the fact that a water molecule has a small moment of inertia because almost all mass is in the oxygen atom and only two light hydrogen atoms are located away from it. This fast convergence means that RD coefficient of water molecules in liquid phase can be obtained within a few picoseconds.

Figure 3 shows the correlations between D_r^{-1} and D_t^{-1}, as well as between D_r^{-1} and viscosity over temperature μ/T in bulk systems at various temperatures. The viscosity is calculated from the off-diagonal component of the pressure tensor, and is expressed in the Einstein form by

$$\mu = \frac{V}{2kT}\lim_{t\to\infty}\frac{1}{t}\left\langle\left(\int_0^t P_{\xi\zeta}(\tau)d\tau\right)^2\right\rangle \quad [\xi,\zeta(\neq\xi) = x,y,z], \tag{8}$$

where V, k, T and $P_{\xi\zeta}$ denote the volume, Boltzmann constant, temperature and an off-diagonal component of the pressure tensor, respectively, whilst brackets denote the spatio-temporal average. The choice $P_{\xi\zeta}$ in Eq. (8) is arbitrary in an equilibrium system as long as directions ξ and ζ are orthogonal, and the average of 6 components in xyz coordinate is used here. The pressure tensor $\boldsymbol{P}$ is calculated by the virial theorem:

$$\boldsymbol{P} = \frac{1}{V}\left(\sum_i m_i \vec{v}_i \otimes \vec{v}_i + \sum_i \sum_{j(>i)} \vec{f}_{ij} \otimes \vec{r}_{ij}\right), \tag{9}$$

where m_i and $\vec{v}_i$ denote mass and velocity of molecule i, respectively, while $\vec{f}_{ij}$ and $\vec{r}_{ij}$ are the force and relative position vectors from i to j, respectively. The summation is taken over all molecules in a system of volume V. As shown by the dotted fitting line in Fig. 3, both D_r^{-1}-D_t^{-1} and D_r^{-1}-μ/T are linearly correlated. These linear correlations indicate that at least in a bulk system D_r may essentially give the same information as D_t and also as viscosity over temperature. The advantage of RD is the ability to obtain a spatial distribution with a higher resolution in a heterogeneous system compared to TD as mentioned above.

Figure 4 shows the temperature dependence of viscosity in the bulk system. The viscosity values derived from the off-diagonal component of the pressure tensor in Eq. (8) as well as ones evaluated from the TD and RD coefficients are depicted along with experimental data [20]. Unknown effective radius values in Eqs. (1) and (2) are set as $R_t = 0.1176$ nm and $R_r = 0.1078$ nm, which are chosen so that the resulting viscosity values correspond to that calculated with the pressure tensor in Eq. (8) at $T = 300$ K. Although the three calculated viscosity values are slightly different from the experimental one because the SPC/E potential is not optimized for the reproduction of viscosity, the temperature dependence is qualitatively well reproduced by the MD simulation. The correspondence among viscosity values calculated using the virial theorem, average TD and RD coefficients at various temperatures reveals that RD coefficient can also adequately reflect viscosity in a bulk system.

Only the bulk average of viscosity is discussed until this part, however, an important target of this study is to relate local distributions of the viscosity to RD coefficient. Regarding local viscosity, Dimitrov et al. [21] evaluated the spatial distribution in a quasi-one-dimensional heterogeneous Lennard-Jones system. In this model, the region is divided into M flat bins parallel

to xy-plane. The local pressure tensor $\boldsymbol{P}^\alpha$ of a bin α is calculated as

$$\boldsymbol{P}^\alpha = \frac{1}{\Delta V}\left(\sum_i m_i \vec{v}_i \otimes \vec{v}_i f^K(z_i) + \sum_i \sum_{j(>i)} \vec{f}_{ij} \otimes \vec{r}_{ij} f^U(z_i, z_j)\right), \tag{10}$$

where ΔV denotes the volume of bin whilst $f^K(z_i)$ and $f^U(z_i, z_j)$ are weighting functions of kinetic and force components, respectively due to molecule i and j with z-coordinates z_i and z_j. See Ref. [21] for the detailed expressions of the weighting functions that distribute each component to bins. Using the local pressure tensor in Eq. (10), the local viscosity μ^α of bin α expressed in the Green-Kubo form is given by

$$\mu^\alpha = \frac{\Delta V}{kT}\sum_{\beta=1}^{M}\int_0^\infty \left\langle P^\alpha_{\xi\zeta}(0) P^\beta_{\xi\zeta}(t)\right\rangle dt, \quad [\xi, \zeta(\neq \xi) = x, y] \tag{11}$$

as the sum of cross correlation integral with all bins β. However, when this original expression is applied to a system which is largely governed by the Coulomb interaction as in our study, the integral in Eq. (11) hardly converges. This is known as 'long tail' [22, 23] and becomes especially remarkable for the cross correlation components with $\alpha \neq \beta$, and also in the case the Green-Kubo form is applied for small bins. As an alternative, we have only extracted the autocorrelation component instead

$$\mu^\alpha_{\mathrm{ac}} = \frac{\Delta V}{kT}\int_0^\infty \left\langle P^\alpha_{\xi\zeta}(0) P^\alpha_{\xi\zeta}(t)\right\rangle dt, \tag{12}$$

which has the largest contribution to the local viscosity μ^α in Eq. (11). Without cross correlation, Eq. (12) can be equivalently rewritten in the Einstein form as

$$\mu^\alpha_{\mathrm{ac}} = \frac{\Delta V}{2kT}\lim_{t\to\infty}\frac{1}{t}\left\langle\left(\int_0^t P^\alpha_{\xi\zeta}(\tau)d\tau\right)^2\right\rangle. \tag{13}$$

We examine here whether an apparent correlation between the average viscosity μ and this viscosity autocorrelation component μ_{ac} calculated with Eqs. (8) and (13), respectively exists in a bulk system. Figure 5 shows the μ-μ_{ac} relation at various temperatures, where μ_{ac} is evaluated for a flat bin with a thickness of 0.26 nm. This thickness is also used for the analysis in Fig. 6, and is described in the next subsection. It is apparent that the two are

linearly correlated, and this indicates that the local viscosity can be evaluated by the viscosity autocorrelation component μ_{ac}. The relation estimated from the dotted fitting line resulted in $\mu_{\mathrm{ac}} = 8.58\mu$. This relation is used for the evaluation of local viscosity in a heterogeneous system described in the next subsection.

3.2. Viscosity distribution in heterogeneous water system between solid walls

As described in the introduction, the RD coefficient changed near the solid surface depending on the surface property in our previous work [11]. According to the Stokes-Einstein-Debye equation in Eq. (2) and the D_r^{-1}-μ relation in Fig. 3, this may have indicated a local change in viscosity. In order to examine the relation between local viscosity and RD coefficient, we have calculated their local distributions in a quasi-one-dimensional equilibrium system of water between solid surfaces as shown in Fig. 1.

Before going to the result, the boundary effect of solid wall should also be mentioned here. The Stokes drag force acting on a sphere translating in a fluid is increased by the presence of a neighboring wall by a factor given by Faxen's correction [24, 25, 26, 27]. However, this is mostly negligible for the rotational motion in the present simulation because the solid-liquid interaction from wall atoms is only imposed on the oxygen. Assuming that a single water molecule is situated on the solid wall, the potential energy does not change even if the orientation of the water molecule changes, provided the position of oxygen atom is kept unchanged. Since the center of mass position of a water molecule is close to the oxygen atom, this means that almost no torque is exerted from the solid wall to reduce the rotation of a water molecule. Hence the boundary condition for the rotational motion there is basically considered as free-slip. **In addition, it is not clear if the linear correlation between the TD and RD coefficients of water molecules in the bulk system also holds for the water near the solid-liquid interface, because the effect of the solid wall on translational and rotational motions may be different. However, as mentioned in the introduction, it is difficult to obtain the spatial distribution of the TD coefficient in a heterogeneous system with a high resolution, because it is evaluated as a position displacement and this means that the position after the displacement is different from the initial one, although the TD value ought to be calculated is that at the initial location. In other words, the resolution of TD coefficient**

distribution is basically comparable to the displacement within the convergence time.

Figure 6 shows the distributions of viscosities in systems of water between solid walls with solid-liquid interaction parameter $\eta = 0.4$, 1.2 and 2.0, where the viscosities are evaluated by means of two methods: 1) $\mu_{\rm ac}$ calculated from the local autocorrelation component using Eq. (13) and μ-$\mu_{\rm ac}$ relation in Fig. 5, and 2) $\mu_{\rm rd}$ calculated using D_r through D_r^{-1}-μ/T relation in Fig. 3. The density distribution is superimposed as well, from which two or three adsorption layers with high density can be observed as distinct peaks. Both $\mu_{\rm ac}$ and $\mu_{\rm rd}$ are calculated for flat bins parallel to the solid wall with a thickness of 0.26 nm, where the thickness is determined so that the density peaks near the solid surface are clearly separated. All data are also averaged from both top and bottom sides taking the symmetry of the system into account, and the temporal average of 24 ns is shown, although a time-averaging this long is only required for the calculation of $\mu_{\rm ac}$; indeed $\mu_{\rm rd}$ has quickly converged within about 100 ps. Although the viscosity value $\mu_{\rm ac}$ does not fully converge even with a time-averaging of 24 ns, both $\mu_{\rm ac}$ and $\mu_{\rm rd}$ are almost constant far from the solid wall independent of solid-liquid interaction parameter η, while they do change near the solid wall depending on it. By comparing both viscosity values in the first adsorption layer, it is obvious that they increase as η increases, and this tendency qualitatively matches for both. However, the two values are quantitatively very different and the correlation between the two does not seem to directly hold in this heterogeneous system.

Regarding the mismatch between $\mu_{\rm ac}$ and $\mu_{\rm rd}$ in Fig. 6, it may be reasonable to take the inhomogeneity of density into account because the density in adsorption layers near the solid wall in Fig. 6 is sensitive to the change in the solid-liquid interface parameter η. When we look again into the Stokes-Einstein-Debye relation in Eq. (2), the RD coefficient D_r is inversely proportional not only to the viscosity μ but also to R^3, and it is fairly probable that this effective radius R depends on the density. Hence, we have assumed here that the cube of radius is inversely proportional to the density ρ, i.e. $R^3 \propto 1/\rho$, which is reasonable considering the relation between molecular volume and density. Figure 7 displays the distribution of ρ/D_r superimposed with that of $\mu_{\rm ac}$ in the same systems as in Fig. 6. The average density of a bin with a thickness of 0.26 nm, in which the $\mu_{\rm ac}$ and D_r distributions are calculated, is applied here. Although there are slight discrepancies, the two distributions show similar tendencies for all η values. The correspondence be-

tween μ_{ac} and ρ/D_r indicates that the one-dimensional viscosity distribution with a spatial resolution of a few angstrom can equivalently be reproduced by means of RD coefficient and density. As mentioned above, it is hard to calculate the viscosity distribution by using the virial theorem for a system largely governed by the Coulomb interaction even through a long temporal average over 20 ns. Meanwhile, the distributions of RD coefficient can easily be calculated because it has a short timescale of several tens of picoseconds, and obtaining the density distribution is also not difficult.

It should also be noted that it is potentially possible to calculate the distribution of RD coefficient not only in a steady state but also in a transient state by taking advantage of its fast-converging feature. **In addition, a simplified system is used at present as the initial step, in which a perfect crystal structure is used as a solid wall and the solid-liquid interaction is represented as the L-J potential between wall and oxygen atoms. However, as a further step, the method shown in this study should be applied to a system with more complex wall structures and with Coulomb interactions between solid and liquid constituent molecules, e.g. a system with a solid surface terminated by hydroxyl groups which form hydrogen bonds with water molecules [28], or one with aqueous solution containing ions in which an electric double layer is formed at the interface.**

4. Concluding remarks

The relation between the RD coefficient of water molecules and viscosity, that theoretically are inversely proportional to each other, was examined by using molecular dynamics simulations. In a homogeneous bulk liquid system, both the viscosity calculated from the virial theorem and experimental one correlated well with the inverse of water RD coefficient at various temperatures. In a heterogeneous system of water between solid walls with different solid-liquid interaction strength, the viscosity distribution was similar to the distribution of inverse of RD coefficient multiplied by density, and this suggests the possibility of extracting nanometer-scale viscosity distribution by RD.

Acknowledgments

Y. Y. is supported for this research by the Ministry of Education, Science, Sports and Culture, Grant-in-Aid for Young Scientists (B), 22760131, 2010,

and Grant-in-Aid for Scientific Research (C), 25420123, 2013.

References

[1] M. Majumder, N. Chopra, R. Andrews, B. J. Hinds, Enhanced flow in carbon nanotubes, Nature 438 (2005) 44–44.

[2] J. K. Holt, H. G. Park, Y. Wang, M. Stadermann, A. B. Artyukhin, C. P. Grigoropoulos, A. Noy, O. Bakajin, Fast mass transport through sub-2-nanometer carbon nanotubes, Science 312 (2006) 1034–1037.

[3] M. Whitby, L. Cagnon, M. Thanou, N. Quirke, Enhanced fluid flow through nanoscale carbon pipes, Nano Lett. 8 (2008) 2632–2637.

[4] J. P. N. G. Hummer, J. C. Rasaiah, Water conduction through the hydrophobic channel of a carbon nanotube, Nature 414 (2001) 188.

[5] A. Alexiadis, S. Kassinos, Molecular simulation of water in carbon nanotubes, Chemical Reviews 108 (2008) 5014–5034.

[6] J. A. Thomas, A. J. H. McGaughey, Reassessing fast water transport through carbon nanotubes, Nano Lett. 8 (2008) 2788–2793.

[7] K. Falk, F. Sedlmeier, L. Joly, R. R. Netz, L. Bocquet, Molecular origin of fast water transport in carbon nanotube membranes: Superlubricity versus curvature dependent friction, Nano Lett. 10 (2010) 4067–4073.

[8] H. Kyakuno, K. Matsuda, H. Yahiro, Y. Inami, T. Fukuoka, Y. Miyata, K. Yanagi, Y. Maniwa, H. Kataura, T. Saito, M. Yumura, S. Iijima, Confined water inside single-walled carbon nanotubes: Global phase diagram and effect of finite length, J. Chem. Phys. 134 (2011) 244501.

[9] L. Bocquet, J. L. Barrat, Infuence of wetting properties on hydrodynamic boundary conditions at a fluid/solid interface, Faraday Discuss 112 (1999) 119–127.

[10] L. Bocquet, J. L. Barrat, Flow boundary conditions from nano- to micro-scales, Soft Matter 3 (2007) 685–693.

[11] D. Surblys, Y. Yamaguchi, K. Kuroda, T. Nakajima, H. Fujimura, Analysis on wetting and local dynamic properties of single water droplet on a polarized solid surface: a molecular dynamics study, J. Chem. Phys. 135 (2011) 014703.

[12] R. F. Probstein, Physicochemical Hydrodynamics, Wiley-Interscience, 1994.

[13] M. G. Mazza, N. Giovambattista, F. W. Starr, H. E. Stanley, Relation between rotational and translational dynamic heterogeneities in water, Phys. Rev. Lett. 96 (2006) 057803.

[14] H. J. C. Berendsen, J. R. Grigera, T. P. Straatsma, The missing term in effective pair potentials, J. Chem. Phys. 91 (1987) 6269–6271.

[15] H. C. Andersen, Molecular-dynamics simulations at constant pressure and-or temperature, J. Chem. Phys. 72 (1980) 2384–2393.

[16] M. Lupkowski, F. Swol, Computer simulation of fluids interaction with fluctuating walls, J. Chem. Phys. 93 (1990) 738–745.

[17] I. P. Omelyan, On the numerical integration of motion for rigid polyatomics: The modified quaternion approach, Computers Phys. 12 (1998) 97–103.

[18] N. S. Martys, R. D. Mountain, Velocity verlet algorithm for dissipative-particle-dynamics-based models of suspension, Phys. Rev. E 59 (1999) 3733–3736.

[19] W. F. van Gunsteren, A. E. Mark, Validation of molecular dynamics simulation, J. Chem. Phys. 108 (1998) 6109–6116.

[20] Chronological Science Tables, Third Edition, National Institutes of Natural Sciences, National Astronomical Observatory of Japan, 2011.

[21] D. Dimitrov, A. Milchev, K. Binder, Local viscosity in the vicinity of a wall coated by polymer brush from green-kubo relations, Macromol. Theory Simul. 17 (2008) 313–318.

[22] Y. Pomeau, P. Re'sibois, Time dependent correlation functions and mode-mode coupling theories, Phys. Rep. 19 (1975) 63–139.

[23] P. Re'sibois, M. de Leener, Classical Kinetic Theory of Fluids, Wiley, New York, 1977.

[24] H. Faxe'n, Der widerstandgegen die bewegung einer starren kugel in einer za:hen flu:ssigkeit die zwischen zwei parallelen ebenen wa:nden eingeschlossen ist,, Ark. Mat. Astron. Fys. 18 (1924) 1–52.

[25] J. Happel, H. Brenner, Low Reynolds Number Hydrodynamics, Kluwer, 1991.

[26] A. Saugey, L. Joly, C. Ybert, J. L. Barrat, L. Bocquet, Diffusion in pores and its dependence on boundary conditions, J. Phys. Condens. Matter 17 (2005) S4075.

[27] E. Lauga, T. M. Squires, Brownian motion near a partial-slip boundary: A local probe of the no-slip condition, Phys. Fluids 17 (2005) 103102.

[28] K. Yamashita, H. Daiguji, Molecular simulations of water adsorbed on mesoporous silica thin films, J. Phys. Chem. C 117 (2013) 2084–2095.

Table 1: Potential and mass parameters, where $\sigma_{\mathrm{wall-wall}}$ is only used for the Lorentz-Berthelot mixing rule $\sigma_{ij} = (\sigma_{ii} + \sigma_{jj})/2$.

$\epsilon_{\mathrm{O-O}}$ (J)	$\epsilon^0_{\mathrm{O-wall}}$ (J)	η	$\sigma_{\mathrm{O-O}}$ (nm)	$\sigma_{\mathrm{wall-wall}}$ (nm)
1.08×10^{-21}	1.247×10^{-21}	0.4−2.0	0.3166	0.35
$\sigma_{\mathrm{O-wall}}$ (nm)	q_{H} (e)	q_{O} (e)	k (N/m)	r_0 (nm)
0.3333	0.4238	−0.8476	46.8	0.277
m_{H} (kg)	m_{O} (kg)	m_{wall} (kg)		
1.674×10^{-27}	2.657×10^{-26}	3.239×10^{-25}		

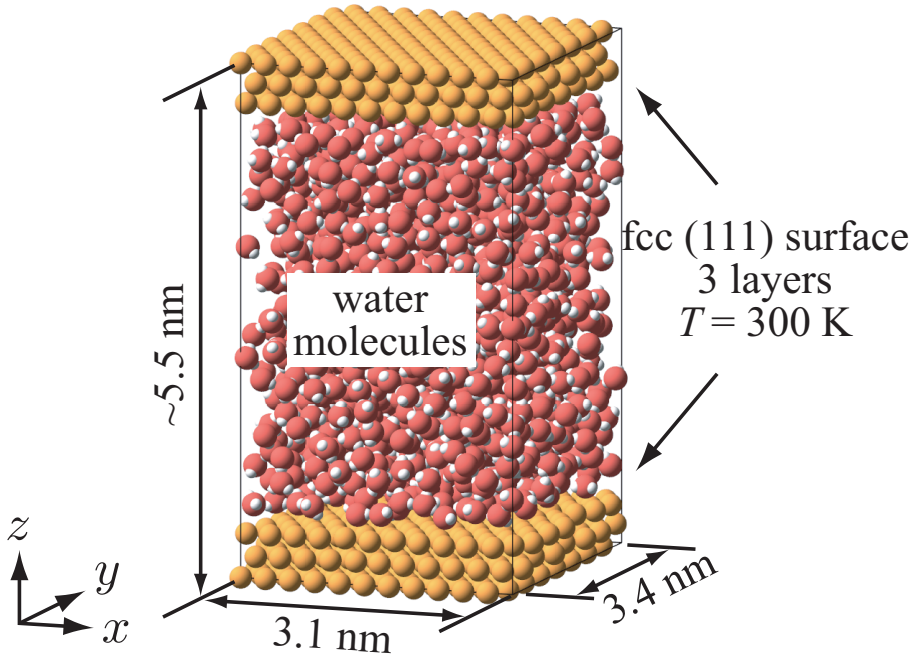

Figure 1: Heterogeneous simulation system of liquid water between solid surfaces. Periodic boundary conditions are imposed in x- and y-directions. The number of water molecules is between 1362 and 1454 depending on the solid-liquid interface parameter η.

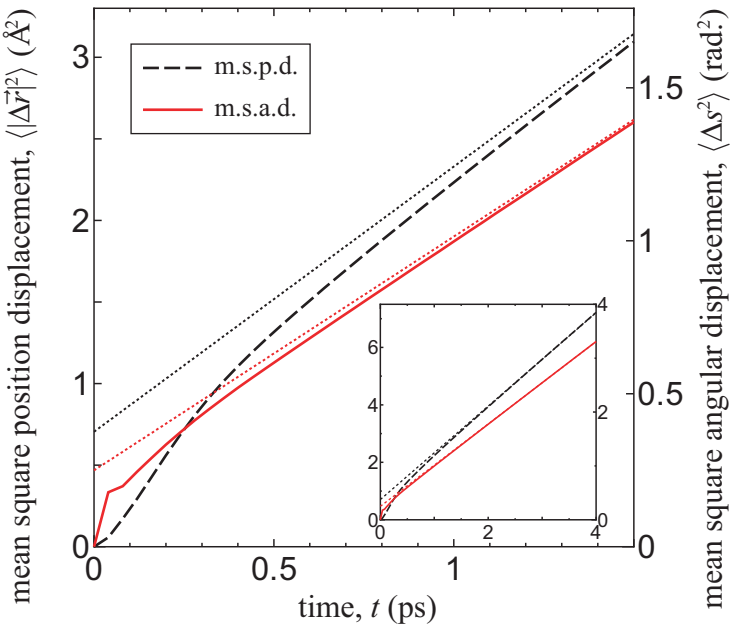

Figure 2: Time development of the mean square position displacement of center of mass and of the mean square angular displacement of principal axes of water molecule in a bulk system at $T = 300$ K. First-order fitting for the range from 2 to 7 ps is shown by the dotted lines.

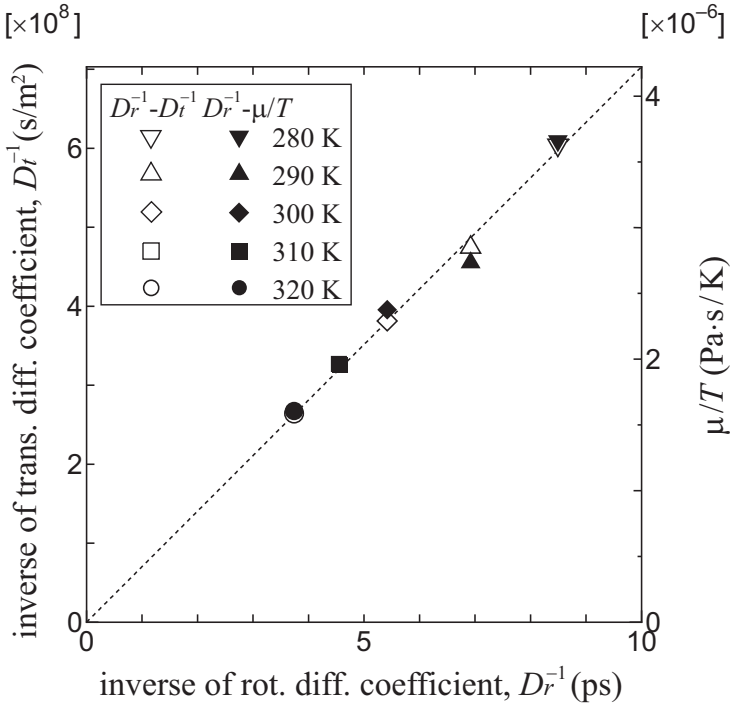

Figure 3: Correlations between inverse rotational diffusion coefficient D_r^{-1} and inverse translational coefficient D_t^{-1} as well as between D_r^{-1} and viscosity over temperature μ/T in bulk systems at various temperatures.

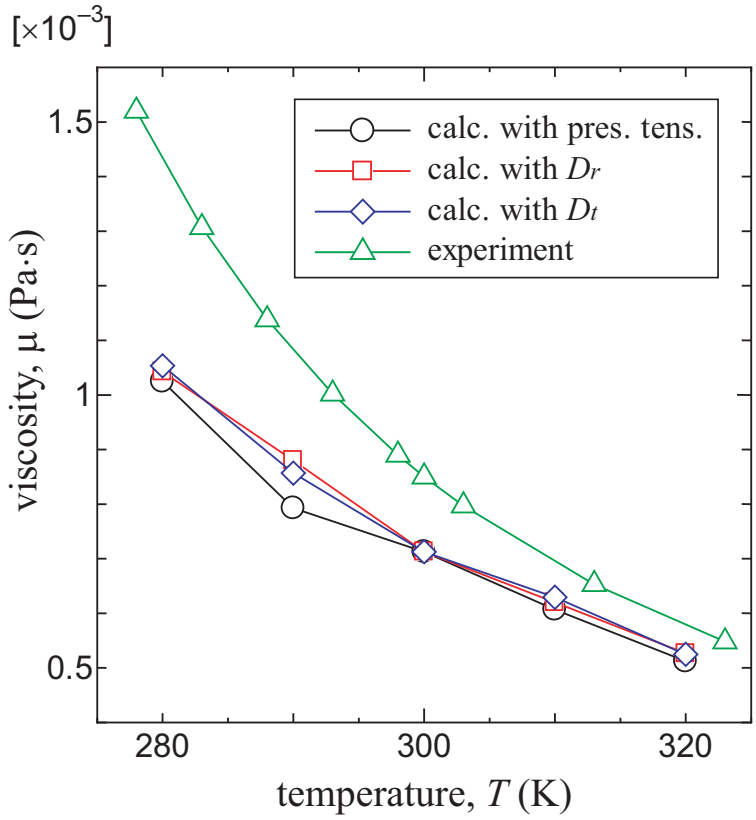

Figure 4: Temperature dependence of viscosity in the bulk system. The viscosity values derived from the off-diagonal component of the pressure tensor in Eq. (8) as well as ones evaluated from the translational and rotational diffusion coefficients are depicted along with the experimental ones [20].

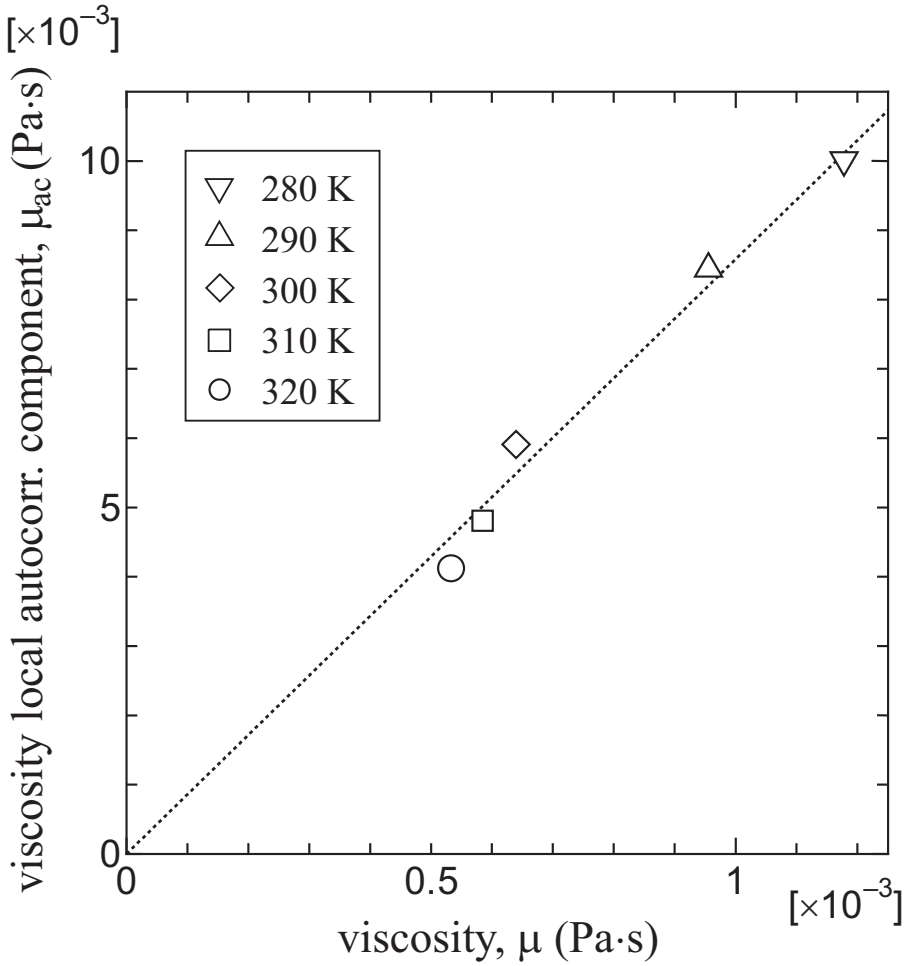

Figure 5: Relation between average viscosity calculated with Eq. (8) and the viscosity local autocorrelation component of a flat bin with a thickness of 0.26 nm calculated with Eq. (13) in bulk systems at various temperatures.

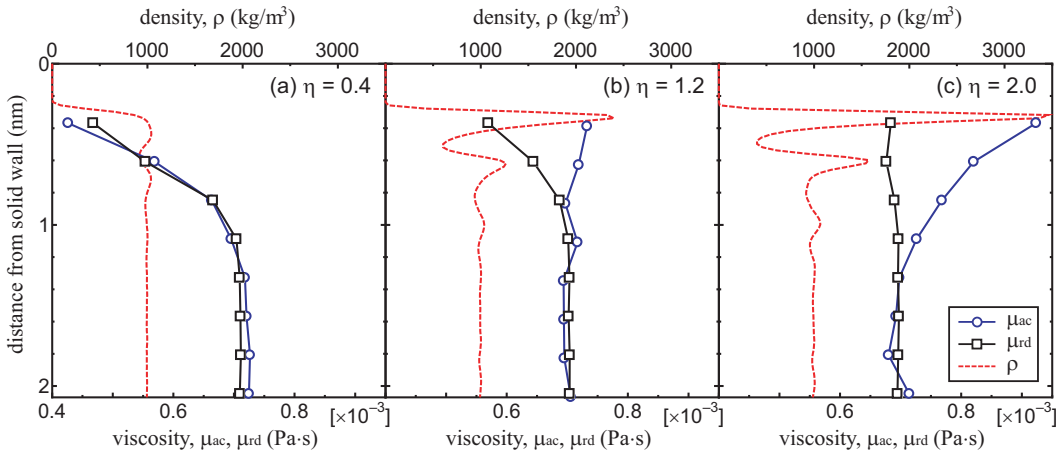

Figure 6: Distributions of viscosities in systems of water between solid walls with solid-liquid interaction parameter $\eta = 0.4$, 1.2 and 2.0. The viscosity is evaluated by means of two methods: 1) $\mu_{\rm ac}$ calculated from the local autocorrelation component using Eq. (13) and μ-$\mu_{\rm ac}$ relation in Fig. 5, and 2) $\mu_{\rm rd}$ calculated using D_r through D_r^{-1}-μ/T relation in Fig. 3. The density distribution is superimposed.

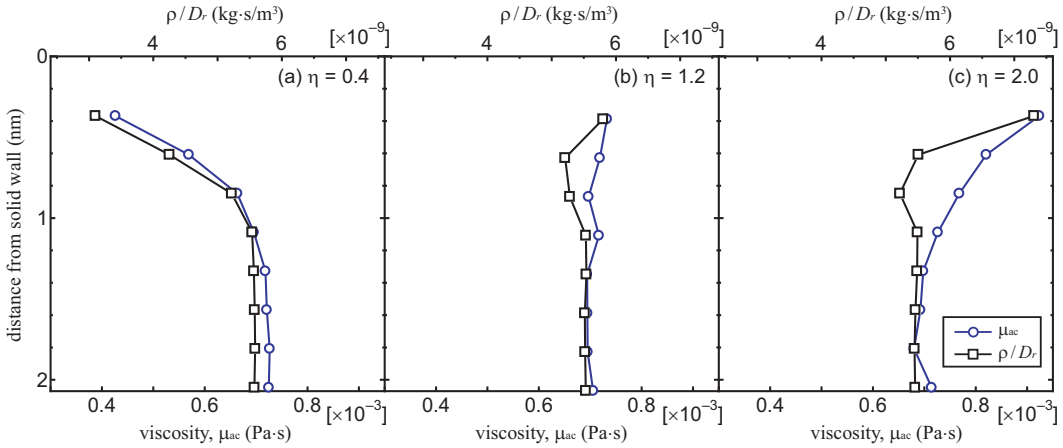

Figure 7: Distribution of ρ/D_r superimposed with that of μ_{ac} in the same systems as in Fig. 6.